LA-6986-MS
Informal Report

UC-21

Issued: October 1977

Structured Pellet Design for Laser Fusion: A Numerical Determination of the Optimum Mass Ratio

Michael A. Stroscio

los alamos
scientific laboratory
of the University of California
LOS ALAMOS, NEW MEXICO 87545

An Affirmative Action/Equal Opportunity Employer

UNITED STATES
DEPARTMENT OF ENERGY
CONTRACT W-7405-ENG. 36

This work was supported by the US Energy Research and Development Administration, Division of Laser Fusion.

Printed in the United States of America. Available from
National Technical Information Service
U.S. Department of Commerce
5285 Port Royal Road
Springfield, VA 22161

Microfiche	$ 3.00	126-150	7.25	251-275	10.75	376-400	13.00	501-525	15.25
001-025	4.00	151-175	8.00	276-300	11.00	401-425	13.25	526-550	15.50
026-050	4.50	176-200	9.00	301-325	11.75	426-450	14.00	551-575	16.25
051-075	5.25	201-225	9.25	326-350	12.00	451-475	14.50	576-600	16.50
076-100	6.00	226-250	9.50	351-375	12.50	476-500	15.00	601-up	--1
101-125	6.50								

1. Add $2.50 for each additional 100-page increment from 601 pages up.

STRUCTURED PELLET DESIGN FOR LASER FUSION: A NUMERICAL DETERMINATION OF THE OPTIMUM MASS RATIO

by

Michael A. Stroscio

ABSTRACT

Structured pellets for laser fusion have been suggested in the past few years. Herein, numerical simulations are presented which demonstrate a departure from purely elastic collisions and illustrate the significance of temporal shaping of the incident laser energy.

Recently, structured pellet designs for attaining laser-produced fusion of deuterium and tritium (DT) have been suggested.[1-4] The basic features of the design proposed in Ref. 4 are shown in Fig. 1 which depicts a section of a spherical laser fusion pellet. The actual dimensions given in Fig. 1 differ from those given in Ref. 4; however, the shell structure is similar - an outer shell of Fe surrounds a cushion material (CH_2) which contains a shell of Au that encloses the DT mixture (frozen onto the inner Au surface with a density of 0.21 g/cm^3).

As indicated in Fig. 1, the laser deposits its energy in the outer Fe shell which is accelerated radially inward and collides with the Au shell. (The low-density CH_2, $\rho = 0.005$ g/cm^3, has low hydrodynamic impedance and has the additional advantages of (1) enhancing the elasticity of the Fe - Au collision and (2) compensating for the lack of perfect symmetry in the imploding Fe shell.) The attractive features of incorporating the Fe shell and CH_2 cushion in the pellet (rather than directly depositing the laser energy in the Au shell) have been addressed in Ref. 4. In that reference, it is shown, assuming certain efficiencies for energy transfer and elastic collisions, that the power, P_2, necessary to result in an energy per unit mass, ε, in the DT and a velocity, v, at the Au - DT interface is given by,

$$P_2 = \frac{(1+r)^3}{8r} \frac{R_{DT-Au}}{\Delta R} P_1 \quad , \tag{1}$$

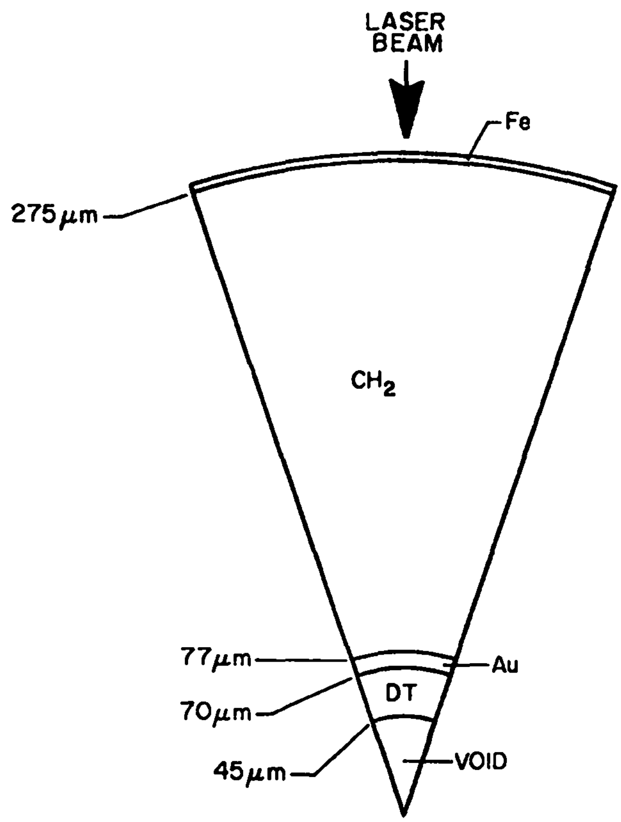

Fig. 1. Section of the spherical laser fusion pellet. The outer radius of the Fe shell is a variable as discussed in the text.

where r is the ratio of the Fe mass to the Au mass, R_{DT-Au} is the radius of the DT-Au interface (at time zero), ΔR is the cushion thickness and P_1 is the power necessary to achieve the same ε and v when the laser deposition occurs directly on the Au shell. From Eq. (1), it follows that $\partial P_2/\partial r = 0$ at $r = 1/2$ and $\partial^2 P_2/\partial r^2 > 0$ for $r \geq 0$; hence, the optimum power P_2 occurs for $r = 1/2$. As noted in Ref. 4, Eq. (1) does not include the effects of shocks and convergence.

Herein numerical simulations are presented which demonstrate that the design of Fig. 1 departs from the purely elastic behavior implicit in Eq. (1). Specifically, the thermonuclear neutron yield has been calculated for the above pellet design with the numerical simulation code LASNEX[5] for (1) several different temporal profiles of the incident laser pulse and (2) values of r between 1/2 and 3/2.

LASNEX is a two-dimensional Lagrangian hydrodynamics code which couples the laser energy to the laser-produced plasma by inverse bremsstrahlung, resonant absorption and instability absorption. In addition, LASNEX incorporates multi-group flux-limited transport of charged particles, multi-group diffusion photonics, three-temperature capability, and thermonuclear burn physics. In the particular calculations presented here the superthermal electron temperature is assumed[6-9] to be proportional to $(I\lambda^2)^{1/4}\, T_e^{1/2}$ where I is the incident laser intensity, λ is the laser wavelength and T_e is the thermal electron temperature.

In the present calculations, three different temporal pulse shapes have been utilized for the incident pulse of 10.6 μm CO_2 light: Pulse A is defined by a temporal profile in which the laser power rises linearly from 0.0 TW at 0.0 ns to 100.0 TW at 2.3 ns and then falls abruptly to 0.0 TW for times greater than 2.3 ns; Pulse B has the same general features as Pulse A with the exception that the peak power is 50.0 TW (instead of 100.0 TW); Pulse C is characterized by a linear rise in power from 0.0 TW at 0.0 ns to 10.0 TW at 0.2 ns followed by a linear drop in power from 10.0 TW at 0.2 ns to 0.0 TW at 2.3 ns. For all three pulses, the power is 0.0 TW before 0.0 ns and after 2.3 ns. In all simulations with these pulses, it is assumed that 50% of the incident CO_2 laser energy is deposited in the outer region of the Fe shell.

Table I summarizes some of the primary results obtained from the LASNEX simulations of the design in Fig. 1 for Pulses A, B, and C. For all of the calculations presented in Table I, the mass of the Au, m_{Au}, is ≃ 9.2 μg and the mass of the DT, m_{DT}, is 0.22 μg. r is the ratio of m_{Fe} to m_{Au}. The values of r are obtained by adjusting the outer radius of the Fe shell in Fig. 1 to give the appropriate mass ratio. N_n is the calculated number of thermonuclear 14 MeV neutrons, τ_{Burn} is the time at which the thermonuclear burn occurs and $E_{Incident}$ is the laser energy incident on the pellet up to the time immediately following thermonuclear burn. (The thermonuclear burn occurs in an approximately 20-ps interval centered at τ_{Burn}.) The values of N_n as a function of r are also depicted in Fig. 2 for Pulses A, B, and C.

Two features are apparent from these results. First, the pulse shape has a pronounced influence on the value of N_n; for example, when r = 3/4 Pulse C results in four times more neutrons than Pulse B for only approximately 1/3 of the incident energy. It is noted parenthetically that there has been no attempt to maximize the value of N_n in this study; however, the above example clearly demonstrates that larger values of N_n may be obtained by varying the temporal shape of the incident pulse. The simulation which gave the maximum value of N_n in Table I had values of "ρR" and T_e of 1.5×10^{-2} g/cm^2 and 400 eV, respectively. It thus follows that the neutron yield could be improved by increasing T_e at the expense of ρR. The second point (which addresses the question of departure from purely elastic behavior implicit in Eq. (1)) is evident upon inspection of Fig. 2. Specifically, for all pulses studied, the value of N_n is strongly peaked at r ≃ 3/4 instead of at r = 1/2 (which is consistent with elastic collisions).

In conclusion, the results of these simulations clearly demonstrate (1) the extreme importance of the temporal shape of the incident laser pulse and (2) that the departures from purely elastic behavior can be quite significant. With regard to this last conclusion, it is noted that for Pulse C nearly 100 times more neutrons result at r ≃ 3/4 than result at r = 1/2 which is the optimum value of r in the context of purely elastic collisions.

TABLE I

SUMMARY OF SIMULATION RESULTS

Pulse	r	N_n	τ_{Burn}(ns)	$E_{Incident}$(kJ)
A	1/2	1.6×10^8	1.20	31.3
A	3/4	2.8×10^9	1.25	34.0
A	1	8.7×10^8	1.30	36.7
A	5/4	3.0×10^8	1.50	48.9
A	3/2	1.8×10^8	1.85	74.4
B	1/2	4.8×10^7	1.50	24.5
B	3/4	4.0×10^8	1.60	27.8
B	1	8.9×10^7	1.80	35.2
B	5/4	5.8×10^7	1.95	41.3
B	3/2	5.3×10^7	2.15	50.2
C	1/2	2.7×10^7	1.60	10.3
C	3/4	1.6×10^9	1.70	10.6
C	1	1.0×10^9	2.00	11.3
C	5/4	4.0×10^8	2.20	~ 11.5
C	3/2	1.7×10^8	2.30	11.5

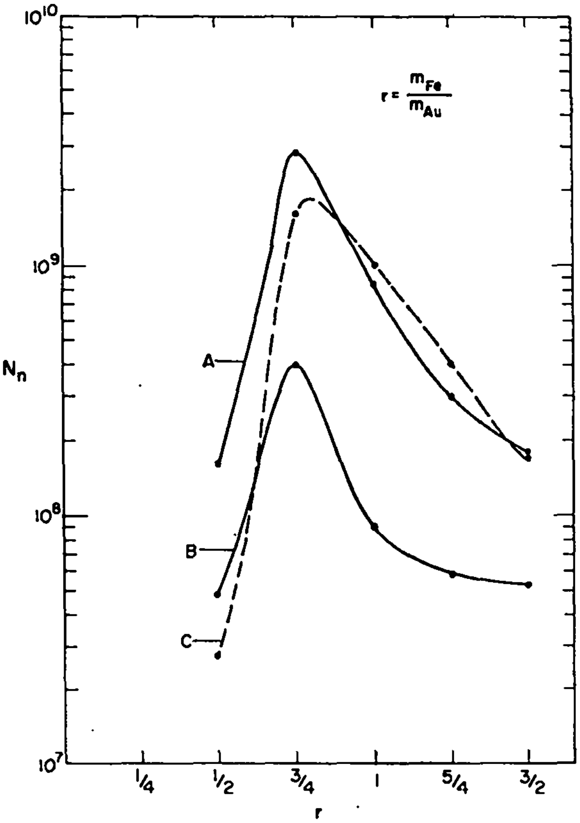

Fig. 2. The calculated number of thermonuclear neutrons, N_n, as a function of the mass ratio, r, for Pulses A, B, and C.

REFERENCES

1. Physics Today 26, 17 (1973).

2. G. Yonas, J. W. Poukey, K. R. Preswich, J. R. Freeman, A. J. Toepfer, M. J. Clauser, Nucl. Fusion 14, 731 (1974).

3. M. J. Clauser, Bull. Am. Phys. Soc. 19, 856 (1974).

4. R. C. Kirkpatrick, C. C. Cremer, L. C. Madsen, H. H. Rogers, and R. S. Cooper, Nucl. Fusion 15, 333 (1975).

5. G. A. Zimmerman, Lawrence Livermore Laboratory Report UCRL-74811 (1973).

6. D. W. Forslund, J. M. Kindel, and K. Lee, Bull. Am. Phys. Soc. 21, 1067 (1976).

7. D. V. Giovanielli, Bull. Am. Phys. Soc. 21, 1047 (1976).

8. D. B. Henderson and M. A. Stroscio, Phys. Rev. Lett. 37, 1244 (1976).

9. M. A. Stroscio, "Theoretical Results Relating Experimental X-Ray Spectra to the Number and Total Energy of Suprathermal Electrons in Laser-Heated Plasmas," Los Alamos Scientific Laboratory report LA-6465-MS (August 1976).